Effect of Intense Weathering and Postdepositional Degradation of Organic Matter on Hg/TOC Proxy in Organic-rich Sediments and its Implicationsfor Deep-Time Investigations

Guillaume Charbonnier, Thierry Adatte, Karl B. Föllmi, Guillaume Suan

Geochemistry, Geophysics, Geosystems

AGU100 ADVANCING EARTH AND SPACE SCIENCE

RESEARCH ARTICLE
10.1029/2019GC008707

Key Points:
- Oxidation of the T-OAE organic-rich deposits has removed a large part of Hg signal
- Degradation of OAE2 organic-matter has largely affected the Rock Eval parameters
- The recorded Hg/TOC ratios do not reflect original Hg signature

Supporting Information:
- Supporting Information S1

Correspondence to:
G. Charbonnier,
guillaume.charbonnier@unil.ch

Citation:
Charbonnier, G., Adatte, T., Föllmi, K. B., & Suan, G. (2020). Effect of intense weathering and postdepositional degradation of organic matter on Hg/TOC proxy in organic-rich sediments and its implications for deep-time investigations. *Geochemistry, Geophysics, Geosystems*, *21*, e2019GC008707. https://doi.org/10.1029/2019GC008707

Received 17 SEP 2019
Accepted 29 OCT 2019
Accepted article online 03 JAN 2020

Effect of Intense Weathering and Postdepositional Degradation of Organic Matter on Hg/TOC Proxy in Organic-rich Sediments and its Implications for Deep-Time Investigations

Guillaume Charbonnier[1], Thierry Adatte[1], Karl B. Föllmi[1], and Guillaume Suan[2]

[1]Institute of Earth Sciences, Géopolis, University of Lausanne, Lausanne, Switzerland, [2]Université de Lyon, UCBL, ENSL, CNRS, LGL-TPE, Villeurbanne, France

Abstract Mercury (Hg) enrichments in sediments are increasingly used as tracer for distal volcanism in deep-time investigations. The impact of changes in organic-matter deposition and preservation on sedimentary Hg sequestration is, however, poorly understood. In this study, we evaluate the potential role of intense weathering and postdepositional organic-matter degradation on the Hg/TOC proxy in sediments. For this, we investigate weathering profiles in organic-rich sediments from lowermost Toarcian sediments (T-OAE; Lafarge cement quarry, France) and organic-rich deposits from the uppermost Cenomanian-lowermost Turonian Bonarelli level (OAE2; Furlo and Monte Velo, Italy; Manilva and El Chorro, Spain). The comparison of Hg data along weathering profiles in lowermost Toarcian sediments indicates that recent intense oxidation of the originally organic-rich deposits has removed up to 89% of the Hg signal. The organic-rich sediments of the Furlo and Manilva sections are characterized by lower Hg/total organic carbon (TOC) ratios, which suggest important Hg scavenging by organic matter (OM) deposition. At the opposite, in equivalent successions, three significant positive Hg/TOC excursions persist at El Chorro and Monte Velo. These samples exhibit low Hydrogen Index (HI) values, which plot in the field of type-III OM. This resulted from postdepositional degradation of marine OM type II to type III, which largely modified the amount and the quality of OM. Consequently, the recorded Hg/TOC ratios do not reflect original Hg drawdown but postdepositional oxidation, suggesting that extreme care is needed in the evaluation of the history of OM preservation when using Hg as a proxy for volcanic activity.

1. Introduction

During the last few years, mercury (Hg) contents have been increasingly used to investigate the complex relationship between environmental change and the intensity and temporal extension of large igneous province (LIP) activity (e.g., Charbonnier et al., 2017; Charbonnier et al., 2018; Charbonnier & Föllmi, 2017; Font et al., 2016; Gong et al., 2017; Grasby et al., 2015; Jones et al., 2017; Percival et al., 2015; Percival et al., 2016; Percival et al., 2017; Sabatino et al., 2018; Sanei et al., 2012; Scaife et al., 2017; Sial et al., 2013; Sial et al., 2014; Sial et al., 2016; Thibodeau et al., 2016). Hg emissions from volcanoes represent an important natural source of Hg to the atmosphere (Pirrone et al., 2010). Due to its relatively long atmospheric residence time (0.5–1 year; Selin et al., 2008; Driscoll et al., 2013), Hg is transported to distal sites in the form of gaseous elemental mercury (Hg^0; Pyle & Mather, 2003; Percival et al., 2015). Recently, Hg enrichments in sediments have been linked to LIP activity in sedimentary successions of end-Ordovician, latest Permian, end-Triassic, Early Toarcian, Valanginian, latest Hauterivian-earliest Aptian, Early Aptian, Aptian/Albian boundary, Cenomanian-Turonian boundary, and end-Cretaceous and Paleocene-Eocene age (Charbonnier et al., 2017; Charbonnier et al., 2018; Charbonnier & Föllmi, 2017; Font et al., 2016; Gong et al., 2017; Grasby et al., 2015; Jones et al., 2017; Keller et al., 2018; Percival et al., 2015; Percival et al., 2017; Sabatino et al., 2018; Sanei et al., 2012; Scaife et al., 2017; Sial et al., 2013; Sial et al., 2014; Thibodeau et al., 2016).

The enrichment of Hg in sediments results from relatively complex processes (Krupp, 1988). Both in marine and in freshwater environments, Hg has a strong affinity for organic matter (OM), which is indicated by significant Hg enrichments in organic-rich deposits in comparison to background sediments (Gehrke et al., 2009; Sanei et al., 2012). Changes in OM deposition affect rates of Hg drawdown (Gehrke et al., 2009; Outridge et al., 2007; Stern et al., 2009). In modern as in ancient sediments, a strong covariation between

Hg and organic carbon enrichments has been observed (Gehrke et al., 2009; Grasby et al., 2013; Outridge et al., 2007; Stern et al., 2009). Consequently, the Hg concentrations are classically normalized against total organic carbon (TOC) contents in order to identify Hg enrichments not directly related to episodes of increased OM preservation (Sanei et al., 2012). In cases where positive excursions in Hg/TOC ratios are correlated with the original Hg records, it is usually concluded that the Hg enrichments are not related to changes in OM deposition alone but rather associated with massive volcanic activity (Charbonnier & Föllmi, 2017; Font et al., 2016; Gong et al., 2017; Percival et al., 2015; Sanei et al., 2012).

However, the application of Hg and Hg/TOC ratio alone as a proxy for volcanic input and its preservation as a primary signal has been challenged in more recent studies. For example, for samples with less than 0.2 wt.% TOC, Hg/TOC ratios are not considered to reflect realistic values (Grasby et al., 2015). Also, authors have cautioned that signals may not be indicative of Hg input at high TOC% (Gerkhe et al., 2009; Charbonnier & Föllmi, 2017). In addition, due to the complexity of the biogeochemical cycle of Hg, local or regional mechanisms such as local high input of clay, thermogenic release from coal and organic rich deposits, massive wildfires and increased soil erosion, and re-emission processes contribute to increase the global pool of Hg in surface reservoirs, which makes it difficult to identify the volcanic source (Bergquist, 2018). Furthermore, mercury is also sensitive to postdepositional processes leading to dissolution-reprecipitation and enrichment (Smit et al., 2016). Recently, Them et al. (2019) showed the complexity of the Hg cycle using a compilation of Hg data during the Toarcian negative carbon isotope event. These authors have shown that Hg/TOC anomalies were restricted to proximal environments, suggesting that these enrichments reflect regional changes in riverine Hg input rather than direct volcanogenic emissions. Similarly, Shen et al. (2019) reported several Hg enrichments in Ordovician/Silurian boundary sections. Despite high Hg/TOC peaks, the Hg signal is mainly associated with pyrite and provide no evidence of any volcanic influence, which demonstrates the importance of evaluating the main host phase of Hg in marine sediments (Shen et al., 2019). For this, Hg isotopes may help to discriminate Hg sources and cycling in marine sediments between volcanic and terrestrial input (Blum et al., 2014; Thibodeau et al., 2016; Grasby et al., 2017; Shen et al., 2019; Them et al., 2019. In this context, the effect of OM degradation on Hg sequestration during burial and exposure remains poorly investigated, and it is yet unclear to which extent the OM preservation history may affect Hg contents in ancient sediments.

The aims of this study are to investigate (i) the potential consequence of intense weathering on Hg sequestration in organic-rich sediments, and more specifically (ii) the effect of OM degradation during burial and re-exposure on the Hg/TOC ratio, which is used as tracer of volcanic activity. For this, we investigate the relationships between the distribution of Hg and the type and nature of OM in organic-rich strata recording the Toarcian Oceanic Anoxic Event (T-OAE) and the Oceanic Anoxic Event 2 (OAE2). These two episodes of severe and global environmental perturbation led to the widespread deposition of laminated organic-rich sediments, which are characterized by high TOC contents of up to 20 and 40wt.% for T-OAE and OAE2, respectively (e.g., Jenkyns, 2010). The record of the T-OAE was studied in lowermost Toarcian sediments of the Lafarge cement quarry (Beaujolais, SE France), where extreme and localized weathering of the organic-rich strata has been reported (Suan et al., 2013). Thus, these strata offer the opportunity to monitor the impact of weathering on Hg concentrations. The uppermost Cenomanian-lowermost Turonian interval, including the OAE2 Bonarelli level and its equivalents, was studied at Furlo (Umbria-Marche Basin), Monte Velo (Trento Plateau), Manilva (Betic Cordillera), and El Chorro (Betic Cordillera). These sections show fundamental differences in abundance, thermal maturity, and OM type, allowing for detailed comparisons between the quality and the quantity of preserved OM and corresponding Hg contents. We discuss the implications of these results for the use of Hg as a tracer of volcanic activity through geological history.

2. Studied Areas

2.1. Lower Toarcian Record

The Lafarge cement quarry in the Beaujolais area (southeastern France) exposes a lower Toarcian-upper Aalenian shallow-water fossiliferous succession (Figure 1). The lowermost Toarcian succession comprises the "Calcaires Jaunes à *Ammonitella*" Formation and the "Marnes inférieures" Formation (Elmi &

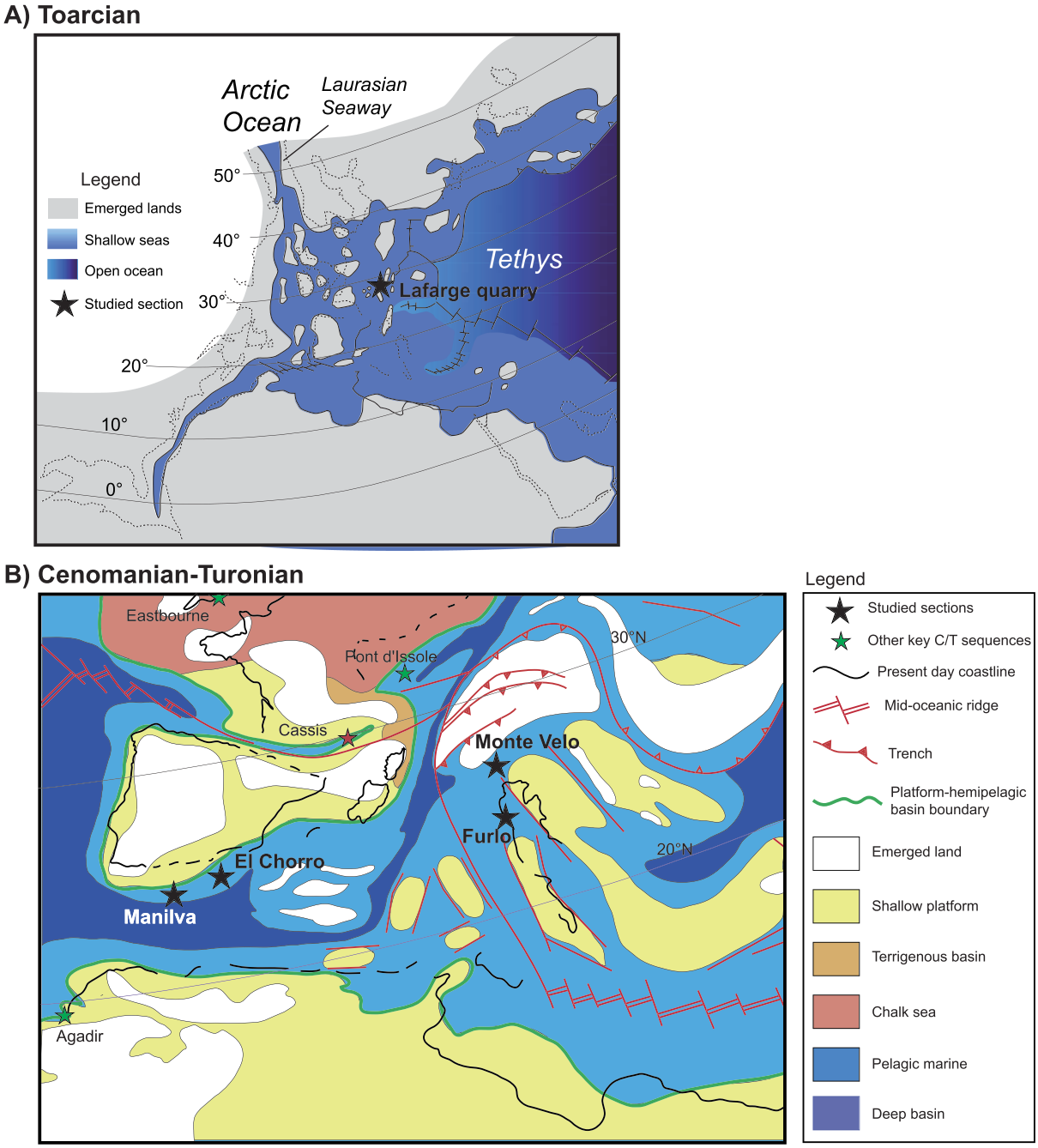

Figure 1. Palaeogeographic map of the western Tethys during the (a) Lower Toarcian (modified from Mattioli et al., 2008) and the (b) uppermost Cenomanian-lowermost Turonian (modified from Dercourt et al., 1993), showing the location of the studied sections (Lafarge cement quarry, Monte Velo, Furlo, Manilva, El Chorro).

Rulleau, 1991). The "Calcaires Jaunes à *Ammonitella*" consists of decimeter-thick, partly dolomitized, calcareous beds interbedded with strongly weathered plastic yellow clays (Figure 2). The nonweathered part of the "Marnes inférieures" is composed of dark gray laminated marls rich in belemnite rostra, whereas the weathered portions are yellow, plastic, and almost structureless (Figure 2). The temporal framework is well defined by ammonites and calcareous nannofossil assemblages (Elmi & Rulleau, 1991; Suan et al., 2013). Furthermore, the lower Toarcian negative carbon isotope excursion is well documented in the inorganic and organic carbon isotope profiles (Suan et al., 2013).

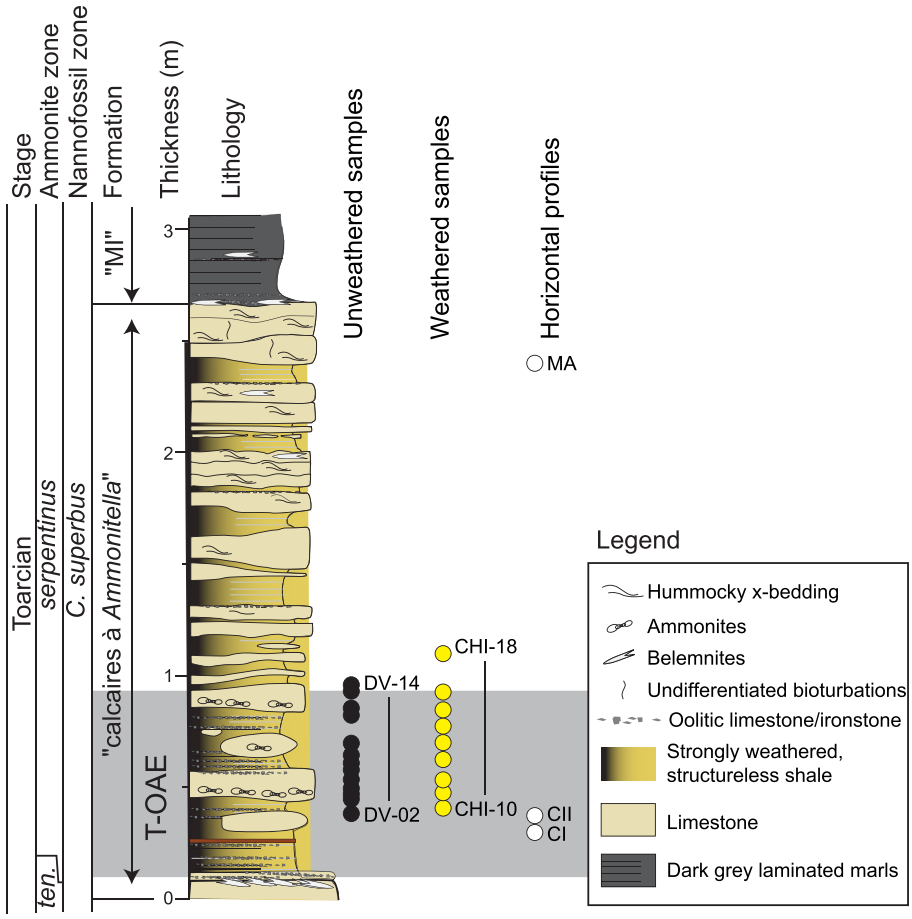

Figure 2. Lithological succession of the Lafarge cement quarry (modified after Suan et al., 2003). The biostratigraphic zonation is based on ammonites and calcareous nannofossils (Suan et al., 2013). Stratigraphic position of the weathered and unweathered bulk rock samples and horizontal profiles are shown.

2.2. Cenomanian-Turonian Boundary Sections

Four sections from the Umbria-Marche Basin (Furlo section, Central Italy), the Trento Plateau (Monte Velo section, northern Italy), and the external Betic Cordillera (El Chorro and Manilva sections, southern Spain), all deposited in pelagic environments, were investigated (Figure 1).

The Umbria-Marche sedimentary basin (Central Italy) was formed during the Late Triassic as a result of extensional tectonics related to the opening of the southern Tethys Ocean (Bertotti et al., 1993). This basin is subdivided into structural highs and basins of varying dimensions and facies. The Furlo section is located in the northern part of the Umbria-Marche Basin. This area is characterized by continuous deposition in a pelagic setting, without any major tectonic disturbance (Arthur & Premoli-Silva, 1982; Bortolotti et al., 1970; Coccioni, 1996). The Trento Plateau (northern Italy) is considered as a paleogeographical-structural unit of the eastern Southern Alps largely affected by postrift thermal subsidence and Alpine compressional tectonics (Bertotti et al., 1993; Winterer & Bosellini, 1981). During the late Jurassic, it was formed as a submarine pelagic plateau surrounded by two basins: the Lombardian Basin to the West and the Belluno Basin to the East (Bosellini et al., 1981). The Monte Velo section is situated in the central-western area of the Trento Plateau. The external Betic Cordillera Zone is composed of a proximal (Prebetic) and a distal basinal (Subbetic) area situated along the southern Iberian paleomargin (Martín-Algarra, 1987; Sanz de Galdeano, 1996). The El Chorro section is located close to the internal-external Betic Cordillera Zone boundary, in the most internal part of the Subbetic Zone, which is also called the Penibetic Zone. This zone consists of the innermost tectonic unit of the external zone of the Betic Cordillera. At the opposite, the Manilva section is situated in the westernmost part of the Subbetic Zone.

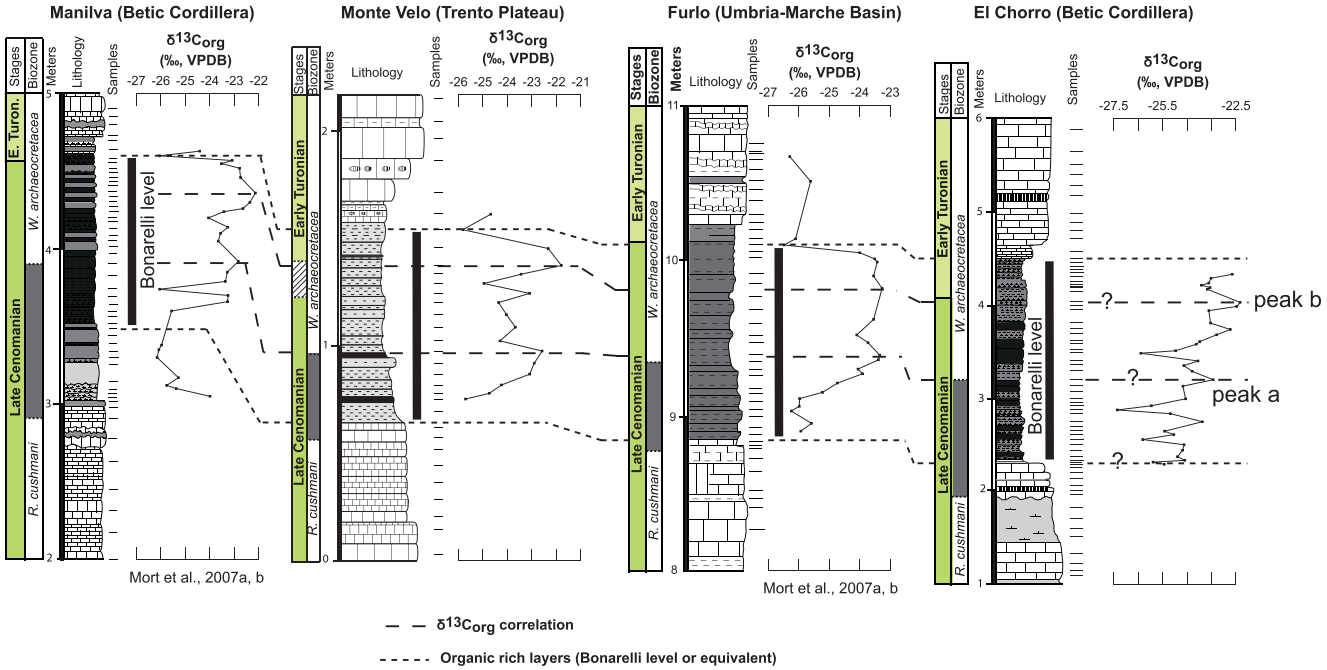

Figure 3. Stratigraphic (short-dashed line) and carbon-isotopic (dashed line) correlations of the Cenomanian/Turonian boundary interval of the Manilva (Subbetic Basin), Monte Velo (Trento Plateau), Furlo (Umbria Marche Basin), and El Chorro (Betic Cordillera) sections (Mort, Jacquat, et al., 2007a, Mort, Adatte, et al., 2007b). The biostratigraphic framework is based on planktonic foraminiferal assemblages (Mort, Jacquat, et al., 2007a, Mort, Adatte, et al., 2007b).

All successions are situated in the same facies zone and are composed of white limestone and mudstone separated by the expression of the Bonarelli level. It consists of an interval between 1 and 2 m thick of laminated organic-rich shale with biogenic phosphate fragments, diatoms, and radiolarian sand (Luciani & Cobianchi, 1999; Figures 3 and 4). These successions of late Cenomanian–early Turonian age are well dated and correlated by planktonic foraminiferal biostratigraphy and carbon-isotope chemostratigraphy (Mort et al., 2007a, Mort et al., 2007b; Figure 3).

3. Material and Methods

3.1. Material

At Lafarge cement quarry, strongly weathered and unweathered, finely laminated organic-rich samples were collected in two sections separated by about 200 m and equivalent in age along the first meter of the "Calcaires Jaunes à *Ammonitella*" Formation, which correspond to the T-OAE (Figure 2). In addition, bulk rock powders were obtained by producing successive, <1-mm-deep trenches on the surface of three slabs using a minidrill equipped with tungsten carbide drill bit. The three slabs correspond to three distinct horizontal horizons (*Harpoceras serpentinus* and *Hildoceras bifrons* ammonite Zones) and show moderately to deeply weathered edges (Figures 2, 5, and 6).

The CT boundary interval at Furlo, Manilva, El Chorro, and Monte Velo was sampled at high resolution, including the organic-rich sediments of the Bonarelli level and its equivalents (Figure 3).

3.2. Methods

A total of 246 samples were measured for their Hg contents, using a Zeeman R-915F (Lumex, St. Petersburg, Russia) high-frequency atomic absorption spectrometer at the University of Lausanne. Analyses are based on the direct thermal evaporation of Hg from solid samples. Measurements were systematically conducted on two aliquots. The accuracy was confirmed by the analysis of certified reference materials (GSD-11 standard, Chinese alluvium: 72.0 ppb; Zintwana et al., 2012) with a correlation coefficient of 0.99 and a standard residual deviation of 5% (±3.6 ppb for the standard). In complement to the Rock-Eval pyrolysis data measured at Manilva and Furlo (Mort et al., 2007a, 2007b), the pyrolysable carbon (PC), the TOC content,

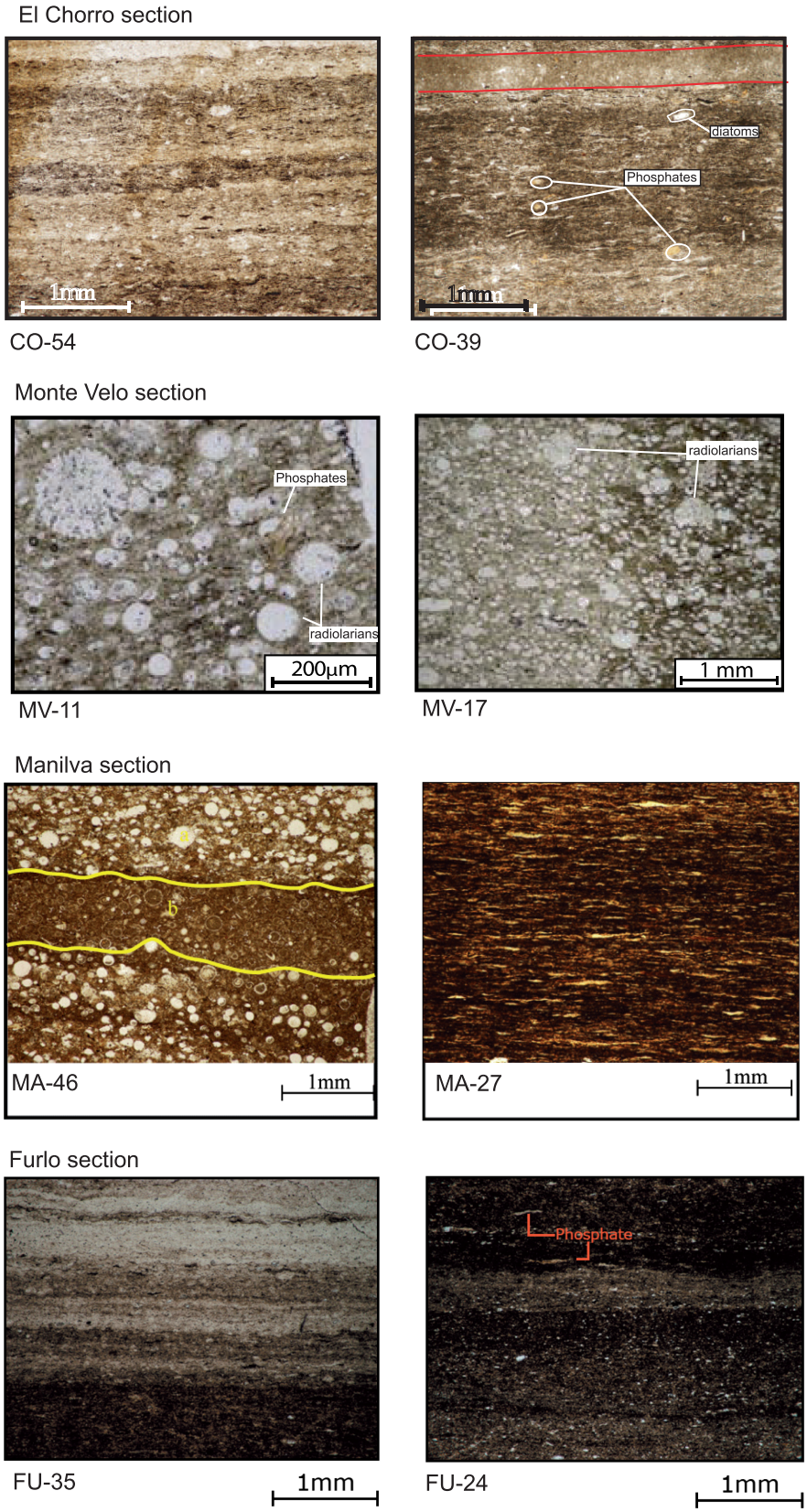

Figure 4. Microfacies photomicrographs of El Chorro, Monte Velo, Manilva, and Furlo sections showing typical laminated organic-rich layers with radiolarians, diatoms, and biogenic phosphate fragments.

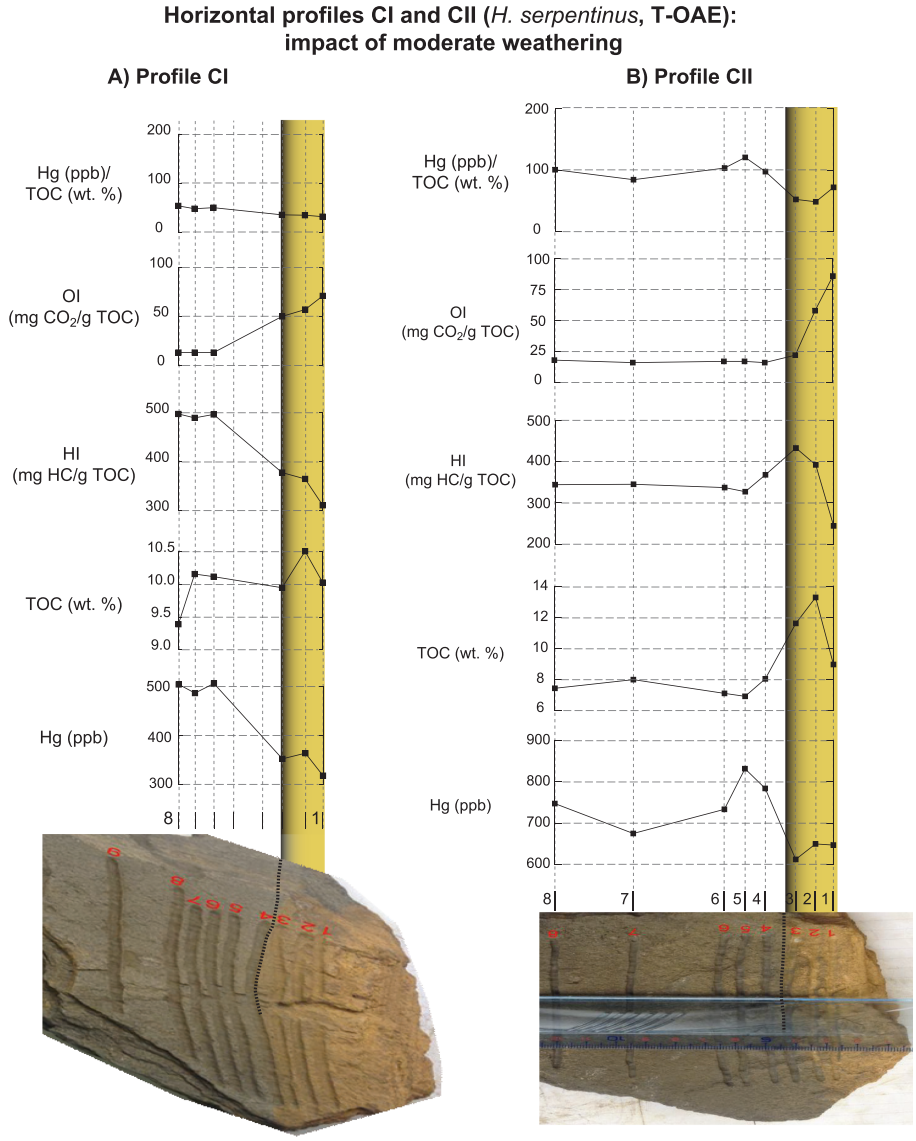

Figure 5. Hg (ppb), TOC (wt.%), HI (mg HC/g TOC), OI (mg CO_2/g TOC), and Hg/TOC (ppb/wt.%) ratios along horizontal profiles (a) CI and (b) CII (*H. serpentinus* ammonite Zone, T-OAE). The yellow bars represent the weathered edges of the horizontal horizons.

hydrogen index (HI), oxygen index (OI), and T_{max} were measured in the samples from the Lafarge cement quarry, El Chorro, and Monte Velo sections using a Rock Eval^{TM} 6 at the University of Lausanne (Behar et al., 2001; Espitalié et al., 1985; Lafargue et al., 1998). Samples were calibrated using the IFP160000 standard with an instrumental precision of <0.1 wt.% for TOC, 1.5 °C for Tmax, 10 mg HC/g TOC for HI, and 10 mg CO_2/g TOC for OI.

4. Results

4.1. Lower Toarcian Sediments

Along the CI, CII, and MA horizontal profiles, the Hg content decreases (from 507 to 317 ppb, from 784 to 647 ppb, and from 578 to 61 ppb, respectively) from the unweathered to weathered bulk rock portions (Figures 5a, 5b, and 6). The organic-carbon record expressed as percent TOC fluctuates between 9.29 and 10.51 wt.% and between 7.09 and 13.30 wt.% in the CI and CII profiles, respectively (Figures 5a and 5b). The OI values vary from 13 to 71 mg CO_2/g TOC and from 17 to 86 mg CO_2/g TOC, and the HI index

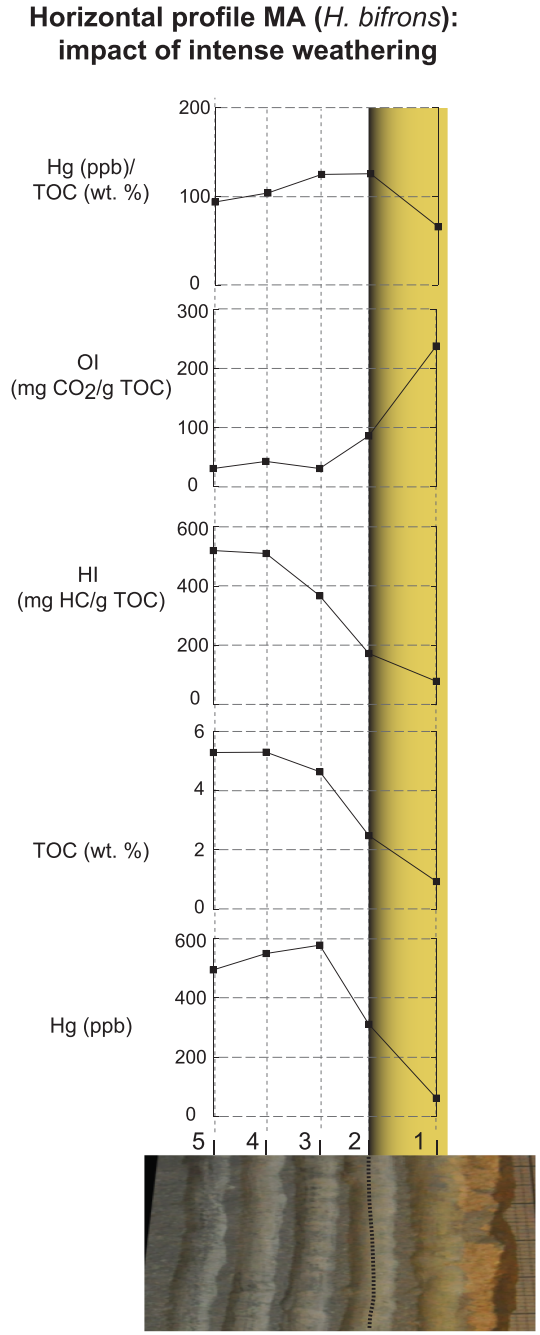

Figure 6. Hg (ppb), TOC (wt.%), HI (mg HC/g TOC), OI (mg CO_2/g TOC), and Hg/TOC (ppb/wt.%) ratios along horizontal profile MA (*H. bifrons* ammonite Zone). The yellow bars represent the weathered edges of the horizontal horizons.

values vary from 498 to 311 mg HC/g TOC and from 433 to 244 mg HC/g TOC, respectively (Figures 5a and 5b). Along the MA horizontal profile, TOC contents are marked by a gradual decrease from 5.3 to 0.93 wt.% from the unweathered to weathered bulk rock portions (Figure 6). The OI values show a significant increase from 31 to 238 mg CO_2/g TOC, and the HI values vary from 520 to 78 mg HC/g TOC (Figure 6). The Hg/TOC ratios in bulk-rock samples along these profiles are characterized by relatively stable values (~100 ppb/wt.%).

The Hg and TOC values measured in strongly weathered and unweathered bulk-rock samples of the T-OAE are plotted in Figure 7. In the section preserving dark gray marl, Hg contents range from 34 to 177 ppb. The TOC values fluctuate between 0.98 and 11.39 wt.% (Figure 7). High TOC values correspond to low OI

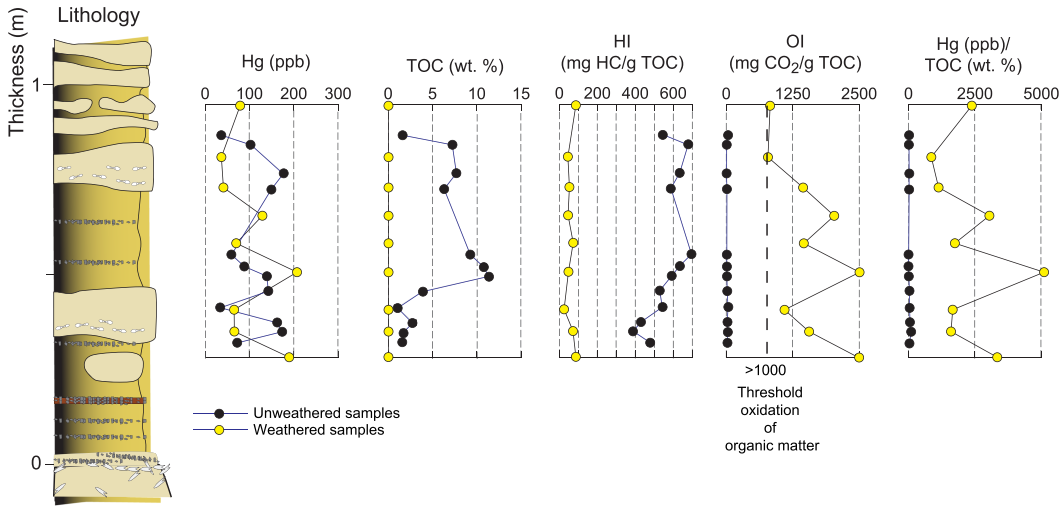

Figure 7. Hg (ppb), Total organic carbon (TOC, wt.%), HI (mg HC/g TOC), OI (mg CO_2/g TOC), and Hg/TOC (ppb/wt.%) ratios data from (a) weathered samples, (b) unweathered samples of the T-OAE interval equivalent.

(<20 mg CO_2/g TOC) and high HI (515–696 mg HC/g TOC) values. The Hg data obtained in the strongly weathered samples show more or less similar values, fluctuating between 65 and 207 ppb. In strong contrast, measured TOC values do not exceed 0.1 wt.% in the same stratigraphic interval in the weathered section (Figure 7). Samples display low HI (<90 mg HC/g TOC) and high OI (up to 2,500 mg CO_2/g TOC) values. The Hg/TOC ratio is rather low and stable in the section preserving dark gray marl, whereas it shows significant high values in weathered sections (up to 5,100 ppb/wt.%).

4.2. Cenomanian-Turonian Boundary Sediments

The Hg records at Furlo, Manilva, Monte Velo, and El Chorro show similarly strong enrichments in the interval corresponding to the Bonarelli level (Figure 8). The Hg variations range from 24 to 233 ppb at Furlo, from 78 to 861 ppb at Manilva, from 13.3 to 394 ppb at Monte Velo, and from 10 to 583 ppb at El Chorro (Figure 8). The Hg values are rather low and stable below and above this interval, not exceeding 40 ppb (Figure 8). The TOC values fluctuate between 0.66 and 17.09 wt.% and between 0.33 and 23.55 wt.% at Furlo and Manilva, respectively (Mort, Jacquat, et al., 2007a, Mort, Adatte, et al., 2007b). High TOC values correspond to low OI (from 21 to 91 mg CO_2/g TOC and from 37 to 105 mg CO_2/g TOC) and high HI (up to 608 and 556 mg HC/g TOC) values (Figure 9). The TOC contents are comparatively moderate at Monte Velo (0.14–1.96 wt.%) and low at El Chorro (0.05–0.94 wt.%; Figure 8). Samples from the Bonarelli equivalent exhibit a low HI (from 49 to 173 mg HC/g TOC and from 3 to 44 mg HC/g TOC) and high OI (up to 463 and 493 mg CO_2/g TOC) values (Figure 9). At Furlo and Manilva, the Hg/TOC ratio displays rather low values along the uppermost Cenomanian-lowermost Turonian interval, fluctuating around 100 ppb/wt. % (Figure 8). In strong contrast at El Chorro and Monte Velo, three significant peaks in the Hg/TOC ratio is observed in the same stratigraphic interval (up to 606 ppb/wt. % at Monte Velo and 1,000 ppb/wt.% at El Chorro; Figure 8).

5. Discussion

5.1. Effect of Surface Weathering on Hg Sequestration

5.1.1. Impact of Moderate to Intense Weathering conditions

The HI (mg HC/g TOC), OI (mg CO_2/g TOC), and TOC (wt.%) values are usually used to estimate the type and quality of preserved OM (Baudin et al., 1998; Espitalié et al., 1985; Hunt, 1995; Suan et al., 2013). High HI values associated to the highest TOC contents indicate a type-II marine OM, which corresponds to a well-preserved OM generally derived from phytoplankton biomass reworked by bacteria. Low HI and high OI values associated with low TOC contents can be a result of a strong alteration of laminated OM (an altered type II).

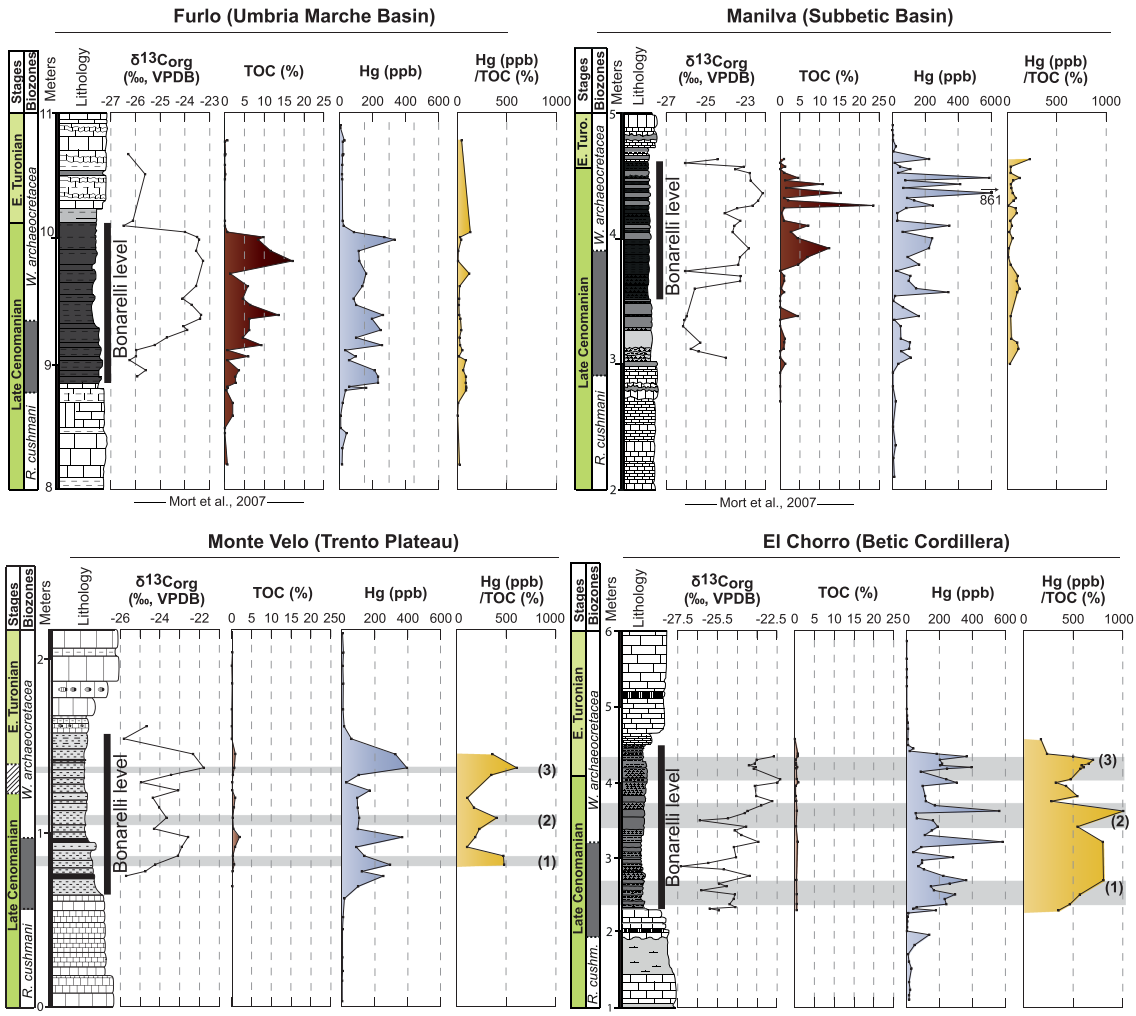

Figure 8. $\delta^{13}C_{org}$ (‰ VPDB), total organic carbon (TOC, wt. %), Hg (ppb), and Hg/TOC (ppb/wt. %) ratios data from Furlo (Central Italy, Umbria Marche Basin), Manilva (southern Spain, Subbetic Basin), El Chorro (southern Spain, Betic Cordillera), and Monte Velo (northern Italy, Trento Plateau) sections. The precise biostratigraphic framework is based on planktonic foraminiferal assemblages (Mort et al., 2007a, 2007b).

A moderate increase in OI (from 13 to 71 mg CO_2/g TOC and from 17 to 86 mg CO_2/g TOC), associated with slightly decreasing HI values (from 498 to 311 mg CO_2/g TOC and from 433 to 244 mg HC/g TOC) is observed in sediments from unweathered to weathered part along the horizontal profiles CI and CII (Figures 5a and 5b). TOC contents show an increase in bulk-rock samples at the beginning of the weathered zone, which is probably related to the disappearance of pyrite while OM is still little oxidized. In the second part of the weathered zone, TOC contents are characterized by slight decrease values (from 10.51 to 10.03 wt. %, and from 13.30 to 8.96 wt.%), which suggests a slight transformation of the original composition and structure of OM related to moderate oxidation. Along these two horizontal profiles, the Hg contents slightly decrease from 499 to 345 ppb (amplitude: 154 ppb) and from 754 to 636 ppb (amplitude: 118 ppb), respectively (Figure 5a and 5b). In strong contrast, along horizontal profile MA (Figure 6), a significant decrease in HI (from 520 to 78 mg HC/g TOC) and TOC (from 5.3 to 0.93 wt.%) values associated with significantly higher OI (from 31 to 238 mg CO_2/g TOC) values indicate poor OM preservation due to intense weathering of the exposure (oxidization). This weathering has led to an important deterioration of the laminated black shales due to intense oxidization. Along the MA horizontal profile, the Hg signal is particularly impacted as is indicated by a dramatic drop in concentrations from 541 to 61 ppb (amplitude: 480 ppb; Figure 6).

Infiltration of meteoric O_2-rich fluids developed during penetration along fault and fracture systems, increasing the permeability and the porosity of the sediment, may have significantly affected the composition and

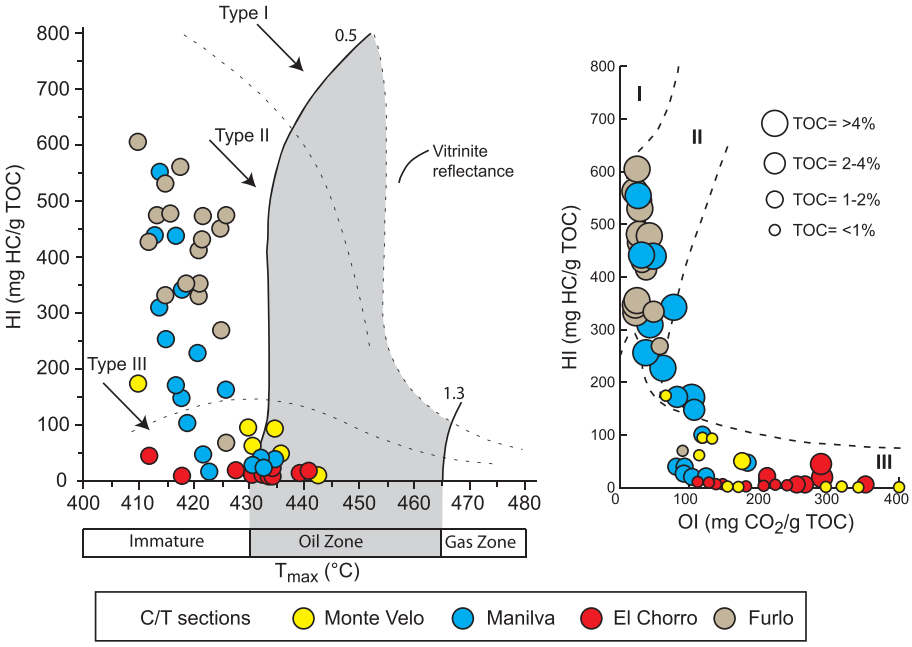

Figure 9. HI/T_{max} diagram for preserved organic matter (OM) and cross plot between Oxygen Index (OI, mg CO_2/g TOC) and Hydrogen Index (HI, mg HC/g TOC) for Furlo, Manilva, Monte Velo, and El Chorro sections in a modified van Krevelen-type diagram, showing the different types of organic matter (Espitalié et al., 1985).

the structure of laminated organic-rich layers (Suan et al., 2013). Differential preservation of the initial structure of laminated organic-rich sequences has led to more or less profound changes in the geochemical characteristics of the succession (Leythäuser, 1973; Littke et al., 1991; Petsch et al., 2000; Suan et al., 2013). Our data suggest that the transformation of both composition and structure of the organic-rich sediments particularly affected the Hg preservation in sediments. Hg element has two common oxidation states: Hg^0 (gaseous species) and Hg^{II} (reactive species). After oxidation to reactive Hg^{II}, Hg is deposited in continental and marine environment by precipitation. In anoxic aquatic environments, dissolved Hg form (Hg^{II}) is methylated by sulfate-reducing bacteria (methylmercury: CH_3Hg^+), which represent the most important mercury species in the environment (Hintelmann, 2010; Parks et al., 2013). Hg methylation processes in sediments can also be controlled by iron-reducing bacteria and methanogens (Fleming et al., 2006; Hamelin et al., 2011). Increase production and bioaccumulation of MeHg forms organo-mercury complexes, which scavenged Hg in bottom sediments and incorporated into long-term geologic storage (e.g., Grasby et al., 2013; Percival et al., 2015). Consequently, dissolved Hg form has a strong affinity for OM and sulfides, which is suggested by a positive correlation between TOC contents and Hg signal (Gehrke et al., 2009; Grasby et al., 2013; Outridge et al., 2007). Thus, destruction of the structure of organic Hg-rich complexes due to infiltration of meteoric O_2-rich fluids affects the overall budget of Hg in the sediments. This is indicated by the fact that between 118 (profile CII: from 754 to 636 ppb), 154 (profile CI: from 499 to 345 ppb) and 480 ppb (profile MA: from 541 to 61 ppb) of the Hg signal was lost due to moderate to intense weathering process, which represents 16%, 31%, and 89% of the unweathered Hg concentrations. However, differential weathering conditions and their impact on the geochemical characteristics of the succession did not cause significant changes in the Hg/TOC ratios, which remain low along the different studied lower Toarcian horizons (Figures 5 and 6).

5.1.2. Impact of Extreme Weathering of Laminated Organic-Rich Sediments

Unweathered finely organic-rich samples corresponding to the T-OAE show high HI (430–696 mg HC/g TOC), low OI (7–34 mg CO_2/g TOC), and the highest TOC (from 0.98 to 11.39 wt.%) values, which are characteristic of good preservation of the marine OM (Figure 7). By contrast, analysis of extremely weathered samples of the same T-OAE horizon reveals that nearly 100% of TOC have been lost (TOC < 0.06 wt.%). The higher OI (785–2,508 mg CO_2/g TOC) and the striking decrease in HI (25–87 mg HC/g TOC) values confirm a high degree of alteration. However, the extremely high OI values reported here have no significance

because they were calculated on extremely low S3 peaks and/or very low TOC values, below the interpretability threshold defined by Espitalié et al. (1985) and Peters (1986). It is also very likely that the presence of carbonate influences the peak S3 during the analysis of these samples, resulting in an extremely strong OI. Intense infiltration of meteoric O_2-rich fluids through fractures and faults contributes to the complete transformation of both composition and structure of the T-OAE organic-rich sediments. Similar changes were observed in Miocene weathering profiles deposited in restricted marine basins off the coast of southern California, where nearly 100% TOC was lost in highly weathered samples (Petsch et al., 2000). Furthermore, it was already demonstrated in the same sediments from the Lafarge quarry that extreme weathering preferentially removed the ^{12}C-enriched organic fraction and induced a severe loss in TOC contents (Suan et al., 2013). The Hg signal is also slightly impacted, as is suggested by the preservation of only one peak in Hg contents in strongly weathered samples (up to 207 ppb) compared to the three peaks recorded in unweathered samples (up to 174, 143, and 177 ppb; Figure 7). This is indicated by the fact that 108 (174 against 66 ppb) and 140 ppb (177 against 37 ppb) of the Hg signal was lost due to the transformation of the structure of the T-OAE organic-rich sediments, which correspond to 62% and 79% of the unweathered Hg concentrations.

Finally, contrary to the first example described above (section 5.1.1), the severe loss in TOC contents had also a severe impact on the Hg/TOC ratios, with the T-OAE weathered samples showing Hg/TOC ratios one to two orders of magnitudes higher (up to 5,000 ppb/wt.%) than unweathered samples (Figure 7). Such values are also orders of magnitude higher than those documented so far for the whole Phanerozoic, which fluctuate between 200 and 800 ppb/wt.% (Charbonnier et al., 2017; Font et al., 2016; Gong et al., 2017; Grasby et al., 2015; Thibodeau et al., 2016). Interestingly, similar Hg/TOC ratios (up to 7102 ppb/wt. %) have been also reported from Frasnian/Famennian sections exposed in desert environment such as in Morocco (Racki et al., 2018), where the composition and structure of organic-rich sediments have very likely been influenced by the development of arid climatic conditions. In this specific environment, the high Hg values (113–1144 ppb) associated with the low TOC contents (0.16–0.67 wt.%) could be in part the expression of the possible influence of surface weathering due to the local climatic conditions. In strong contrast, coeval sites in Germany or in Russia record moderate Hg/TOC peaks of 300 and 100 ppb/wt.% (Racki et al., 2018). Consequently, sediment samples must be carefully screened for the possible influence of surface weathering before to use their Hg/TOC ratios as a tracer of volcanic activity.

5.2. Impact of Postdepositional Degradation of OM on Hg/TOC ratios

In comparison to the Hg contents, the Hg/TOC ratios of the organic-rich deposits of the Furlo and Manilva sections (OAE2) show low and constant background values (from 13.5 to 129.0 ppb/wt. % and from 5.3 to 47.6 ppb/wt.%, respectively), which suggest strong covariation of Hg and OM deposition (Figure 8). The high HI values at Furlo (70–608 mg HC/g TOC) and Manilva (21–556 mg HC/g TOC) indicate that preserved OM is mainly of marine origin (type II OM; Mort et al., 2007b; Figure 8). Moreover, the T_{max} values (405–433 °C and 413–441 °C) indicate that the OM is immature to early mature, suggesting that these sections were not the subject of intense burial diagenesis (Mort, Jacquat, et al., 2007a, Mort, Adatte, et al., 2007b; Figure 9). Furthermore, the higher correlation coefficient between HI values and TOC contents ($R^2 = +0.61$; $n = 40$) and between PC and TOC contents ($R^2 = +0.93$; $n = 80$; Figures 10a and 11) indicate a fairly good OM preservation (Mort et al., Mort, Adatte, et al., 2007b). This is also supported by robust correlation between S2 and S3 peaks ($R^2 = +0.88$; $n = 35$), which represent the amounts of hydrocarbons and oxygen-containing compounds (CO_2) that are produced during the thermal cracking of the insoluble OM in the rocks (Lafargue et al., 1998). In reducing environments, this type of OM is generally derived from phytoplankton biomass reworked by bacteria (including cyanobacteria, iron-reducing bacteria, and methanogens; Tissot & Welte, 1984).

In the aquatic system, a number of processes affects dissolved Hg^{2+}. Especially, in an oxygen-deficient water column, the formation of organo-mercury complexes is generated by anaerobic microorganisms (Hamelin et al., 2011; Lin et al., 2012; Wood et al., 1968), which explains the higher Hg concentrations recorded through the OAE2 interval (up to 332.6 and 860.7 ppb at Furlo and Manilva; Figure 8). The positive correlation between Hg (ppb) and HI (mg HC/g TOC; $R^2 = +0.45$; $n = 40$; Fig. 10b) and between Hg (ppb) and TOC

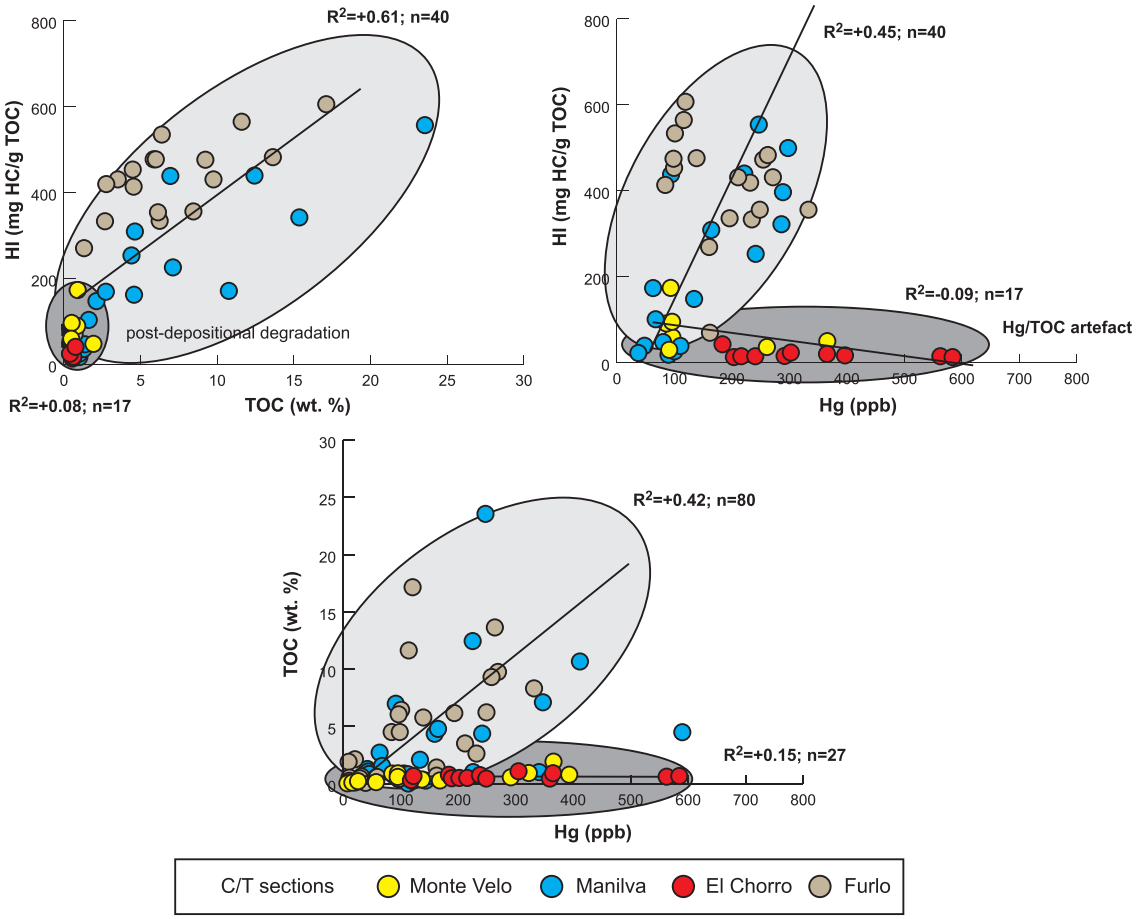

Figure 10. (a) TOC (wt.%) versus HI (mg HC/g TOC), (b) HI (mg HC/g TOC) versus Hg (ppb), and (c) TOC (wt.%) versus Hg (ppb) diagrams for the samples from Furlo, Manilva, Monte Velo, and El Chorro.

(wt.%; $R^2 = 0.42$; $n = 80$; Fig. 10c) at Furlo and Manilva supports this relationship. This is also shown by the Hg/TOC ratios, which remain flat (<150 ppb/wt.%) through the interval (Figure 8).

However, three significant and correlatable excursions in the Hg/TOC ratios (peaks 1, 2, and 3) persist in the Bonarelli level at El Chorro (up to 800, 1,000, and 700 ppb/wt. %, respectively) and Monte Velo (up to 470, 401, and 606 ppb/wt.%, respectively; Figure 8). These excursions are similar if not considerably higher in amplitude than the positive Hg/TOC excursions associated with (i) Hg anomalies during three subsequent extinction events in the Permian/Triassic boundary interval (up to 300 ppb/wt.%; Grasby et al., 2015), (ii) mercury anomalies observed during the end-Ordovician mass extinction (up to 300 ppb/wt. %; Gong et al., 2017), and (iii) mercury anomalies related to the end-Triassic mass extinction (up to 600 ppb/wt. %; Thibodeau et al., 2016). In strong contrast to Furlo and Manilva, preserved OM of the Bonarelli level interval at El Chorro and Monte Velo are characterized by low PC (<0.17 wt.%), and HI values (<174 mg HC/g TOC) and by high OI values (66.7–493 mg CO_2/g TOC) suggesting a terrestrial origin (OM of type III) or an altered type-II (Espitalié et al., 1985; Fig. 9). In addition, the TOC contents at Monte Velo (up to 1.96 wt.%) and El Chorro (up to 0.78 wt.%) are also significantly lower than the organic carbon contents at Furlo (up to 17.10 wt.%) and Manilva (up to 23.55 wt.%). The S2 peak, corresponding to the hydrocarbons generated from kerogen cracking between 300 and 650 °C, appears also very low in the samples (<1.51 mg HC/g; Figure 11).

The Bonarelli level at El Chorro and Monte Velo was deposited in a pelagic environment characterized by organic facies similar to Furlo and Manilva where preserved OM is of explicit marine origin (type II). Moreover, the Bonarelli level deposits consist of laminated sediments rich in radiolaria, diatoms with high amounts of biogenic phosphate fragments, and pyrite (Figure 4). There is no evidence (such as the presence of wood fragments) for the presence of terrestrial OM (Figure 4). Furthermore, in comparison to the two

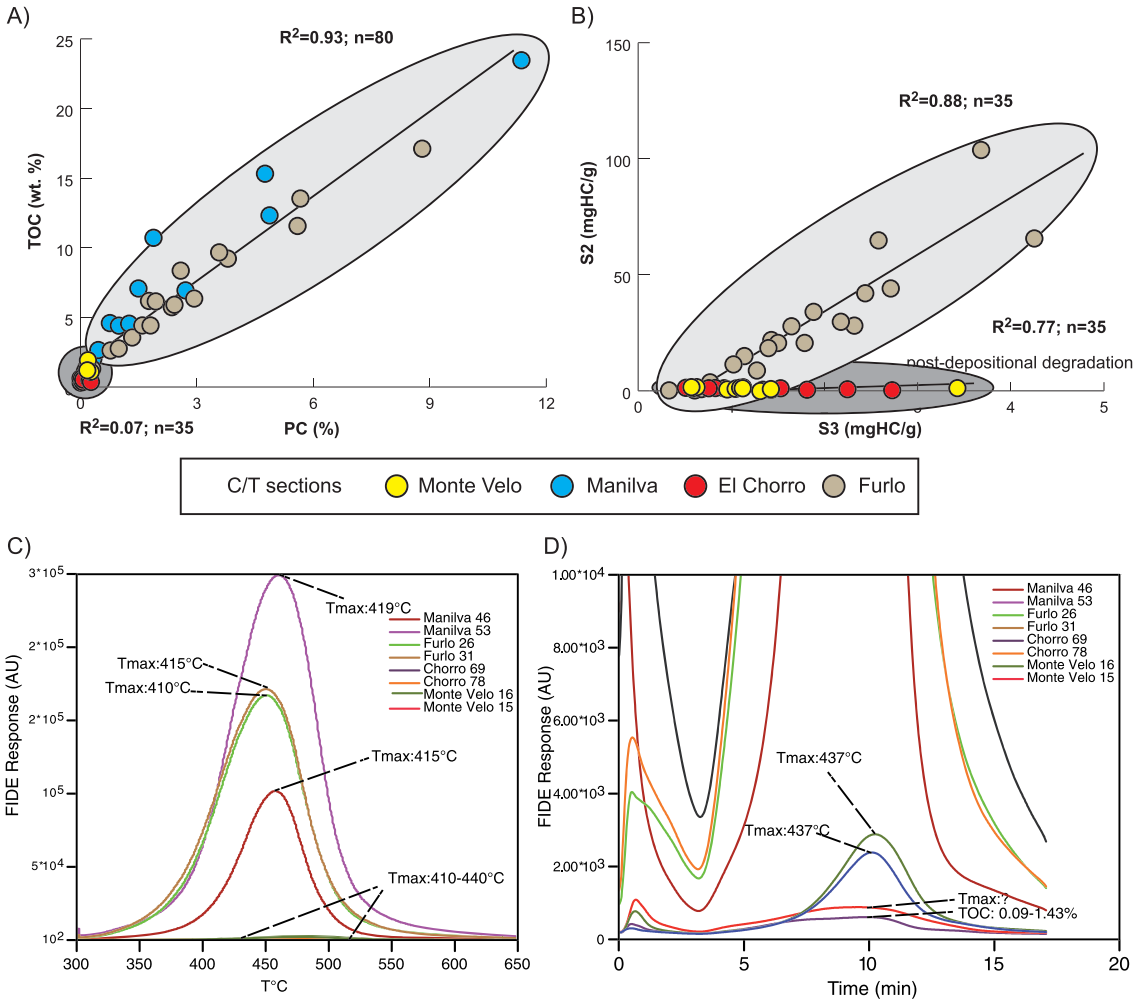

Figure 11. (a) TOC (wt.%) versus PC (%) diagram, (b) S2 (mg HC/g) versus S3 (mg HC/g) diagram, and (c) and (d) S2 thermogram for the samples from Furlo, Manilva, Monte Velo, and El Chorro.

other sections, similar Hg fluctuations have been recorded at Monte Velo and El Chorro, which suggests also a strong influence of biotic processes (i.e., anaerobic microorganisms) during OM deposition. Thus, despite the high Hg values, Hg contents correlate poorly with HI values ($R^2 = -0.09$; $n = 17$) and TOC contents ($R^2 = +0.15$; $n = 27$; Figure 10b and 10c). Contrary to Manilva, the El Chorro section is situated in the most internal part of the Penibetic Zone, in the innermost tectonic unit of the external zone of the Betic Cordillera (Martín-Algarra, 1987; Sanz de Galdeano, 1996). Similarly, contrary to the Umbria-Marche Basin, the Trento Plateau is considered as a paleogeographical-structural unit of the eastern southern Alps that has been largely affected by postrift thermal subsidence and Alpine compressional tectonics (Bertotti et al., 1993; Winterer & Bosellini, 1981). Curiously, the organic-rich samples display T_{max} values between 410 and 443 °C (average 430 °C), which would indicate that these sections were not subjected to intense burial diagenesis (Espitalié et al., 1985). The T_{max} values, corresponding to the temperature at which the maximum rate of hydrocarbon occurred during cracking of kerogen, are measured at the top of S2 peak. At Furlo and Manilva, the intensity and the shape of the S2 peak allow to precisely establish the temperature at the peak top (Figure 11). However, at Monte Velo and El Chorro, the S2 peaks are not well expressed and relatively flat, making interpretation of the resulting T_{max} data more difficult (Figure 11). Consequently, the measured T_{max} values cannot be used to evaluate the maturation of the OM.

The shape of the Rock-Eval thermogram and the low PC and HI values recorded at Monte Velo and El Chorro reflect a high degree of postdepositional degradation of OM that probably reached the oil window (Figure 11). This significantly affected PC, S2 peak, TOC, and HI values by degradation (Figures 9–11),

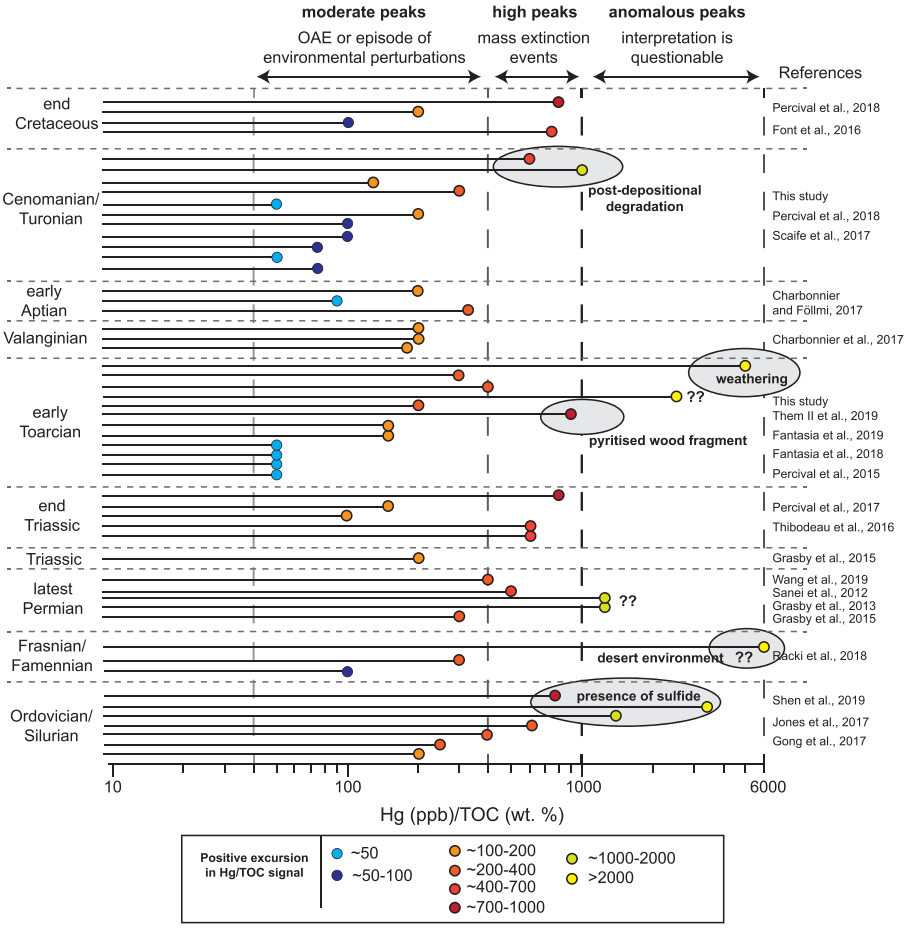

Figure 12. Reported Hg/TOC ratios across various events during the Phanerozoic time interval. The vertical dash lines represent the thresholds between anomalous (>1,000 ppb/wt.%), high (400–1,000 ppb/wt.%), and moderate (<400 ppb/wt.%) Hg/TOC ratio peaks.

but did apparently not influence the Hg signal adsorbed onto OM. This interpretation is well supported by the low HI values and TOC contents in comparison to the same stratigraphic interval at Manilva and Furlo and by the poor correlation between TOC and HI (R^2 = +0.08; n = 17) and between TOC and PC (R^2 = +0.07; n = 35; Figures 10a and 11). Consequently, positive Hg/TOC excursions at El Chorro and Monte Velo persist in sediments during the OAE2 interval (Figure 8). Thus, we interpret the observed high Hg/TOC ratios as a preservational artifact, suggesting that Hg/TOC ratios may be not used alone, but in complement to other information such as the type and the thermal maturation of OM obtained by Rock Eval analyses, especially for deep-time investigations.

5.3. Establishment of Thresholds for Hg Investigations

Positive excursions in Hg/TOC ratios recorded in sedimentary successions have been used to investigate the link between LIPs and environmental perturbations during the Phanerozoic (e.g., Sanei et al., 2012; Grasby et al., 2015; Percival et al., 2015, Percival et al., 2016, Percival et al., 2017; Font et al., 2016; Charbonnier et al., 2017; Gong et al., 2017; Wang et al., 2019; Figure 12). High peaks in Hg/TOC ratios (between 400 and 800 ppb/wt.%) took place during end-Permian, end-Triassic, and end-Cretaceous interval (Sanei et al., 2012; Grasby et al., 2015; Font et al., 2016; Percival et al., 2017, 2018; Figure 12), which correspond to three of the five largest Phanerozoic biodiversity depletions. These anomalous Hg levels may be attributed to the catastrophic Siberian Traps, CAMP volcanism, and Deccan Traps eruptions, which are known as the largest igneous events in Earth history. In contrast, moderate Hg/TOC excursions (up to 400 ppb/wt.%) were restricted only to a few locations during the early Toarcian, early Aptian, and Cenomanian/Turonian oceanic anoxic events (Scaife et al., 2017; Percival et al., 2018; Them et al., 2019; Figure 12). The early Aptian and

Cenomanian/Turonian events were related to the emplacement of submarine LIPs (Ontong Java, Caribbean, and High Arctic). Scaife et al. (2017) suggest that transport by marine currents may explain the smaller Hg concentrations recorded during the OAE1a and OAE2 events (from 50 to 200 ppb/wt.%), compared to the large increases in Hg/TOC ratios related to aerial flux of Hg emitted by continental LIPs (Figure 12). Them et al. (2019) showed the complexity of the Hg cycle using a compilation of Hg data during the Toarcian negative carbon isotope event. These authors have shown that Hg/TOC anomalies were restricted to proximal environments, suggesting that these enrichments reflect regional changes in riverine Hg input rather than direct volcanogenic emissions. However, extreme peaks in Hg/TOC ratios (>1,000 ppb/wt.%) have been also associated with the Ordovician/Silurian, Frasnian/Famennian, early Toarcian, and Cenomanian/Turonian sediments (Figure 12). It has been demonstrated that these excursions are link to the presence of Hg-rich sulfides (Hg/TOC ratio up to 3,400 ppb/wt.%; Shen et al., 2019), the presence of pyritized wood fragments (Hg/TOC ratio up to 900 ppb/wt.%; Fantasia et al., 2019), the impact of extreme weathering of laminated organic-rich sediments (Hg/TOC ratio up to 5,000 ppb/wt.%; this study), the impact of postdepositional degradation of OM (Hg/TOC ratio up to 1,000 ppb/wt.%; this study), and the influence of modern climatic conditions in desert environment (Hg/TOC ratio up to 6,000 ppb/wt.%; Racki et al., 2018). Consequently, for future interpretations, we propose to define thresholds below which any interpretation of these values is questionable (Figure 12). For the extreme Hg/TOC peaks between 1,000 and 6,000 ppb/wt.%, it is necessary to evaluate primary mechanisms leading to Hg accumulation in sediments when using Hg as a proxy for volcanic activity.

6. Conclusions

The Hg contents in lowermost Toarcian sediments of the Lafarge cement quarry and in four sections equivalent to the uppermost Cenomanian-lowermost Turonian interval reveal that weathering and postdepositional degradation of OM may have dramatic consequences on the sedimentary Hg content and hence alter its reliability as a distal tracer of volcanism.

The Hg contents in the Lafarge cement quarry indicate that the intense oxidation of the originally organic-rich laminated sediments has removed a large part of the Hg content (up to 89%). Extreme weathering conditions in the same site led to an almost complete loss of the original TOC content (from 5–10 to 0.06 wt.%) without considerably affecting Hg contents, resulting in anomalously high Hg/TOC ratios in the weathered samples.

The good correlation between Hg and TOC contents in OAE2 organic-rich deposits at Furlo and Manilva, and the resulting invariant Hg/TOC trends, indicate that sedimentary Hg contents are mainly reflecting preferential scavenging during episodes of poor oxygenation and enhanced preservation of type-II OM of marine origin. The Hg contents show similar values for the same interval in the thermally more mature successions at Monte Velo and El Chorro, but correlate poorly with TOC values that are distinctly lower than in the two other OAE2 sites, resulting in three distinctive positive Hg/TOC excursions to anomalously high values. These low TOC contents, together with the flat shape of S2 peak diagram, the low HI, and moderate to high OI values, indicate the dominance of type-III OM, which likely resulted from the strong postdepositional degradation from originally immature type-II OM. These results imply that the degradation and intense weathering of OM has severely affected the Rock Eval parameters but not the Hg signal acquired through biotic processes onto OM when deposited in sediments. Although mechanisms through which Hg is transferred from organic particles to the sedimentary mineral matrix remain poorly constrained, our results clearly demonstrate that Hg/TOC ratios may be strongly impacted by both postdepositional and oxidative degradation of OM, suggesting that a careful evaluation of the quality of preserved OM is crucial when exploring deep-time Hg signatures as a proxy of distal volcanism.

Acknowledgments
We acknowledge the Swiss National Science Foundation (project 200021_168994) and University of Lausanne for financial and logistic support and the association Paleorhodania and Lafarge Val d'Azergues for logistical support during fieldwork in Beaujolais. We would also like to thank Géraldine Paratte, Stéphane Affolter, Pascale Ducommun, and Olivier Jacquat for their initial research, collection of samples in the field, and Rock-Eval analysis. The data which were used to generate the study results are available as supporting information, Data Information S1 and archived in the PANGAEA data repository at https://doi.pangaea.de/10.1594/PANGAEA.909060. We would also like to acknowledge the help of editor Adina Paytan and the constructive comments of François Baudin and one anonymous reviewer.

References

Arthur, M., & Premoli-Silva, I. (1982). Development of widespread organic rich strata in Mediterranean Tethys. In A. Schlanger & M. B. Cita (Eds.), *Nature and origin of Cretaceous carbon-rich facies* (pp. 7–54). London/New York/Paris: Academic Press.

Baudin, F., Fiet, N., Coccioni, R., & Galeotti, S. (1998). Organic matter characterisation of the Selli Level (Umbria-Marche Basin, central Italy). *Cretaceous Research*, *19*(6), 701–714. https://doi.org/10.1006/cres.1998.0126

Behar, F., Beaumont, V., De, B., & Penteado, H. L. (2001). Rock-Eval 6 technology: Perfomances and develoments. *Oil and Gas Science and Technology revue IFP*, *56*(2), 111–134. https://doi.org/10.2516/ogst:2001013

Bergquist, B. A. (2018). Mercury, volcanism, and mass extinctions. *Proceedings of the National Academy of Sciences of the United States of America*, *114*, 8675–8677.

Bertotti, G., Picotti, V., Bernoulli, D., & Castellarin, A. (1993). From rifting to drifting: tectonic evolution of the South-Alpine upper crust from the Triassic to the Early Cretaceous. *Sedimentary Geology*, *86*(1-2), 53–76. https://doi.org/10.1016/0037-0738(93)90133-P

Blum, J. D., Sherman, L. S., & Johnson, M. W. (2014). Mercury isotopes in earth and environmental sciences. *Annual Review of Earth and Planetary Sciences*, *42*(1), 249–269. https://doi.org/10.1146/annurev-earth-050212-124107

Bortolotti, V., Passerini, P., Sagri, M., & Sestini, G. (1970). The miogeosynclinal sequences. *Sedimentary Geology*, *4*(3-4), 341–444. https://doi.org/10.1016/0037-0738(70)90019-9

Bosellini, A., Masetti, D., & Sarti, M. (1981). A Jurassic "Tongue of the Ocean" infilled witth oolitic sands: The Belluno Trough, Venetian, Alps, Italy. *Marine Geology*, *44*(1-2), 59–95. https://doi.org/10.1016/0025-3227(81)90113-4

Charbonnier, G., & Föllmi, K. B. (2017). Mercury enrichments in lower Aptian sediments support the link between Ontong Java large igneous province activity and oceanic anoxic episode 1a. *Geology*, *1*, 63–66.

Charbonnier, G., Godet, A., Bodin, S., Adatte, T., & Föllmi, K. B. (2018). Mercury anomalies, volcanic pulses, and drowning episodes along the northern Tethyan margin during the latest Hauterivian-earliest Aptian. *Palaeogeography, Palaeoclimatology, Palaeoecology*, *505*, 337–350. https://doi.org/10.1016/j.palaeo.2018.06.013

Charbonnier, G., Morales, C., Duchamp-Alphonse, S., Westermann, S., Adatte, T., & Föllmi, K. B. (2017). Mercury enrichments indicate volcanic triggering of Valanginian environmental change. *Scientific Reports*, *7*(1), 1, 40808–6. https://doi.org/10.1038/srep40808

Coccioni, R. (1996). The Cretaceous of the Umbria-Marche Apennines (central Italy), Wiedmann symposium cretaceous stratigraphy, paleobiology and paleobiogeography, the Umbria–Marche Apennines (Central Italy). *Tübingen*, 7-10.

Dercourt, J., Ricou, L. E., & Vrielynck, B. (1993). *Atlas Tethys Paleoenvironmental maps*. Rueil-Malmaison, France: BEICIP–FRANLAB.

Driscoll, C. T., Mason, R. P., Chan, H. M., Jacob, D. J., & Pirrone, N. (2013). Mercury as a global pollutant: Sources, pathways, and effects. *Environmental Science & Technology*, *47*(10), 4967–4983. https://doi.org/10.1021/es305071v

Elmi, S., & Rulleau, L. (1991). Le Toarcien des carrières Lafarge (Bas-Beaujolais, France): un cadre biostrati- graphique de référence pour la région Lyonnaise. *Geobios*, *24*(3), 315–331. https://doi.org/10.1016/S0016-6995(09)90011-0

Espitalié, J., Deroo, G., & Marquis, F. (1985). La pyrolyse Rock-Eval et ses applications. *Revue l'Institut Français du Pétrol*, *40*(5), 563–579. https://doi.org/10.2516/ogst:1985035

Fantasia, A., Adatte, T., Spangenberg, J. E., Font, E., Duarte, L. V., & Föllmi, K. B. (2019). Global versus local processes during the Pliensbachian-Toarcian transition at the Peniche GSSP, Portugal: A multi-proxy record. *Earth Science Reviews*, *198*, 102932. https://doi.org/10.1016/j.earscirev.2019.102932

Fleming, E. J., Mack, E. E., Green, P. G., & Nelson, D. C. (2006). Mercury methylation from unexpected sources: Molybdate-inhibited freshwater sediments and an iron-reducing bacterium. *Applied and Environmental Microbiology*, *72*(1), 457–464. https://doi.org/10.1128/AEM.72.1.457-464.2006

Font, E., Adatte, T., Sial, A. N., de Lacerda, L. D., Keller, G., & Punekar, J. (2016). Mercury anomaly, Deccan volcanism, and the end-Cretaceous mass extinction. *Geology*, *44*(2), 171–174. https://doi.org/10.1130/G37451.1

Gehrke, G. E., Blum, J. D., & Meyers, P. A. (2009). The geochemical behaviour and isotopic composition of Hg in a mid-Pleistocene western Mediterranean sapropel. *Geochimica et Cosmochimica Acta*, *73*(6), 1651–1665. https://doi.org/10.1016/j.gca.2008.12.012

Gong, Q., Wang, X., Zhao, L., Grasby, S. E., Chen, Z. Q., Zhang, L., et al. (2017). Mercury spikes suggest volcanic driver of the Ordovician-Silurian mass extinction. *Scientific Reports*, *7*(1), 5304. https://doi.org/10.1038/s41598-017-05524-5

Grasby, S. E., Beauchamp, B., Bond, D. P. G., Wignall, P., & Sanei, H. (2015). Mercury anomalies associated with three extinction events (Capitanian crisis, latest Permian extinction and the Smithian/Spathian extinction) in NW Pangea. *Geological Magazine*, *13*.

Grasby, S. E., Sanei, H., Beauchamp, B., & Chen, Z. H. (2013). Mercury deposition through the Permo-Triassic biotic crisis. *Chemical Geology*, *351*, 209–216. https://doi.org/10.1016/j.chemgeo.2013.05.022

Grasby, S. E., Shen, W., Yin, R., Gleason, J. D., Blum, J. D., Lepak, R. F., et al. (2017). Isotopic signatures of mercury contamination in latest Permian oceans. *Geology*, *45*(1), 55–58. https://doi.org/10.1130/G38487.1

Hamelin, S., Amyot, M., Barkay, T., Wang, Y., & Planas, D. (2011). Methanogens: Principal methylators of mercury in lake periphyton. *Environmental Science & Technology*, *45*(18), 7693–7700. https://doi.org/10.1021/es2010072

Hintelmann, H. (2010). Organomercurials: Their formation and pathways in the environment. *Metal Ions in Life Sciences*, *7*, 365–401. https://doi.org/10.1039/BK9781847551771-00365

Hunt, J. M. (1995). *Petroleum Geochemistry and Geology* (2nd ed., pp. 408–411). San Francisco: Freeman.

Jenkyns, H. C. (2010). Geochemistry of oceanic anoxic events. *Geochemistry, Geophysics, Geosystems*, *11*(3), Q03004. https://doi.org/10.1029/2009GC002788

Jones, D. S., Martini, A. M., Fike, D. A., & Kaiho, K. (2017). A volcanic trigger for the Late Ordovician mass extinction? Mercury data from south China and Laurentia. *Geology*, *45*(7), 631–634. https://doi.org/10.1130/G38940.1

Keller, G., Mateo, P., Punekar, J., Khozyem, H., Gertsch, B., Spangenberg, J., et al. (2018). Environmental changes during the Cretaceous-Paleogene mass extinction and Paleocene-Eocene Thermal Maximum: Implications for the Anthropocene. *Gondwana Research*, *56*, 69–89. https://doi.org/10.1016/j.gr.2017.12.002

Krupp, R. (1988). Physicochemical aspects of mercury metallogenesis. *Chemical Geology*, *69*(3-4), 345–356. https://doi.org/10.1016/0009-2541(88)90045-9

Lafargue, E., Marquis, F., & Pillot, D. (1998). Rock Eval 6 applications in hydrocarbon exploration production and soils contamination studies. *Oil & Gas Science and Technology*, *53*, 421–437.

Leythäuser, D. (1973). Effects of weathering on organic matter in shales. *Geochimica et Cosmochimica Acta*, *37*, 120–133.

Lin, C.-C., Yee, N., & Barkay, T. (2012). Microbial transformations in the mercury cycle. In G. Liu, Y. Cai, & N. O'Driscoll (Eds.), *Environmental chemistry and toxicology of mercury* (pp. 155–191). Hoboken, NJ: John Wiley & Sons, Inc.

Littke, R., Klussman, U., Krooss, B., & Leythäuser, D. (1991). Quantification of loss of calcite, pyrite and organic matter during weathering of Toarcian black shales and effects on kerogen and bitumen characteristics. *Geochimica et Cosmochimica Acta*, *55*(11), 3369–3378. https://doi.org/10.1016/0016-7037(91)90494-P

Luciani, V., & Cobianchi, M. (1999). The Bonarelli Level and other black shales in the Cenomanian-Turonian of the northeastern Dolomites (Italy): Calcareous nannofossil and foraminiferal data. *Cretaceous Research*, *20*(2), 135–167. https://doi.org/10.1006/cres.1999.0146

Martín-Algarra, A. (1987). Evolución geológica alpina del contacto entre las Zonas Internas y las Zonas Externas de la Cordillera Bética. PhD Thesis, Universidad de Granada, Spain, 1171 pp.

Mattioli, E., Pittet, B., Suan, G., & Mailliot, S. (2008). Calcareous nannoplankton changes across the early Toarcian oceanic anoxic event in the western Tethys. *Paleoceanography*, *23*(3). https://doi.org/10.1029/2007PA001435

Mort, H., Jacquat, O., Adatte, T., Steinmann, P., Föllmi, K., Matera, V., et al. (2007). The Cenomanian/Turonian anoxic event at the Bonarelli Level in Italy and Spain: enhanced productivity and/or better preservation? *Cretaceous Research*, *28*(4), 597–612. https://doi.org/10.1016/j.cretres.2006.09.003

Mort, H. P., Adatte, T., Föllmi, K. B., Keller, G., Steinmann, P., Matera, V., et al. (2007). Phosphorus and the roles of productivity and nutrient recycling during oceanic anoxic event 2. *Geology*, *35*(6), 483–486. https://doi.org/10.1130/G23475A.1

Outridge, P. M., Sanei, H., Stern, G. A., Hamilton, P. B., & Goodarzi, F. (2007). Evidence for control of mercury accumulation rates in Canadian High Arctic lake sediments by variations of aquatic primary productivity. *Environmental Science & Technology*, *41*(15), 5259–5265. https://doi.org/10.1021/es070408x

Parks, J. M., Johs, A., Podar, M., Bridou, R., Hurt, R. A. Jr., Smith, S. D., et al. (2013). The genetic basis for bacterial mercury methylation. *Science*, *339*(6125), 1332–1335. https://doi.org/10.1126/science.1230667

Percival, L. M. E., Cohen, A. S., Davies, M. K., Dickson, A. J., Hesselbo, S. P., Jenkyns, H. C., et al. (2016). Osmium isotope evidence for two pulses of increased continental weathering linked to Early Jurassic volcanism and climate change. *Geology*, *44*(9), 759–762. https://doi.org/10.1130/G37997.1

Percival, L. M. E., Jenkyns, H. C., Mather, T. A., Dickson, A. J., Batenburg, S. J., Ruhl, M., et al. (2018). Does large igneous province volcanism always perturb the mercury cycle? Comparing the records of oceanic anoxic event 2 and the end-Cretaceous to other Mesozoic events. *American Journal of Science*, *318*(8), 799–860. https://doi.org/10.2475/08.2018.01

Percival, L. M. E., Ruhl, M., Hesselbo, S. P., Jenkyns, H. C., Mather, T. A., & Whiteside, J. H. (2017). Mercury evidence for pulsed volcanism during the end-Triassic mass extinction. *PNAS*. https://doi.org/10.1073/pnas.1705378114

Percival, L. M. E., Witt, M. L. I., Mather, T. A., Hermoso, M., Jenkyns, H. C., Hesselbo, S. P., et al. (2015). Globally enhanced mercury deposition during the end-Pliensbachian extinction and Toarcian OAE: A link to the Karoo–Ferrar large igneous province. *Earth and Planetary Science Letters*, *428*, 267–280. https://doi.org/10.1016/j.epsl.2015.06.064

Petsch, S. T., Berner, R. A., & Eglinton, T. I. (2000). A field study of the chemical weathering of ancient sedimentary organic matter. *Organic Geochemistry*, *31*(5), 475–487. https://doi.org/10.1016/S0146-6380(00)00014-0

Pirrone, N., Cinnirella, S., Feng, X., Finkelman, R. B., Friedli, H. R., Leaner, J., et al. (2010). Global mercury emissions to the atmosphere from anthropogenic and natural sources. *Atmospheric Chemistry and Physics Discussions*, *10*(2), 4719–4752. https://doi.org/10.5194/acpd-10-4719-2010

Pyle, D. M., & Mather, T. A. (2003). The importance of volcanic emissions for the global atmospheric mercury cycle. *Atmospheric Environment*, *37*(36), 5115–5124. https://doi.org/10.1016/j.atmosenv.2003.07.011

Racki, G., Rakocinski, M., Marynowski, L., & Wignall, P. B. (2018). Mercury enrichments and the Frasnian-Famennian biotic crisis: A volcanic trigger proved? *Geology*, *46*(6), 543–546. https://doi.org/10.1130/G40233.1

Sabatino, N., Ferraro, S., Coccioni, R., Bonsignore, M., Del Core, M., Tancredi, V., & Sprovieri, M. (2018). Mercury anomalies in upper Aptian-lower Albian sediments from the Tethys realm. *Palaeogeography, Palaeoclimatology, Palaeoecology*, *495*, 163–170. https://doi.org/10.1016/j.palaeo.2018.01.008

Sanei, H., Grasby, S. E., & Beauchamp, B. (2012). Latest Permian mercury anomalies. *Geology*, *40*(1), 63–66. https://doi.org/10.1130/G32596.1

Sanz de Galdeano, C. (1996). The E-W segments of the contact between the external and internal zones of the Bettic and rif cordilleras and the E-W corridors of the internal zone (a combined explanation). *Estudios Geológicos*, *52*, 123–136.

Scaife, J. D., Ruhl, M., Dickson, A. J., Mather, T. A., Jenkyns, H. C., Percival, L. M. E., et al. (2017). Sedimentary mercury enrichments as a marker for submarine Large Igneous Province volcanism? Evidence from the Mid-Cenomanian Event and Oceanic Anoxic Event 2 (Late Cretaceous). *Geochemistry, Geophysics, Geosystems*, *18*(12), 4253–4275. https://doi.org/10.1002/2017GC007153

Selin, N. E., Jacob, D. J., Yantosca, R. M., Strode, S., Jaeglé, L., & Sunderland, E. M. (2008). Global 3-D land-ocean-atmosphere model for mercury: Present-day versus preindustrial cycles and anthropogenic enrichment factors for deposition. *Global Biogeochemical Cycles*, *22*, 1–13.

Shen, J., Algeo, T. J., Chen, J., Planavsky, N. J., Feng, Q., Yu, J., & Liu, J. (2019). Mercury in marine Ordovician/Silurian boundary sections of South China is sulfide-hosted and non-volcanic in origin. *Earth and Planetary Science Letters*, *511*, 130–140. https://doi.org/10.1016/j.epsl.2019.01.028

Sial, A. N., Chen, J., Lacerda, L. D., Frei, R., Tewrai, V. C., Pandit, M. K., et al. (2016). Mercury enrichment and Hg isotopes in Cretaceous-Paleogene boundary successions: Links to volcanism and palaeoenvironmental impacts. *Cretaceous Research*, *66*, 60–81. https://doi.org/10.1016/j.cretres.2016.05.006

Sial, A. N., Chen, J., Lacerda, L. D., Peralta, S., Gaucher, C., Frei, R., et al. (2014). High-resolution Hg chemostratigraphy: A contribution to the distinction of chemical fingerprints of the Deccan volcanism and Cretaceous-Paleogene Boundary impact event. *Palaeogeography, Palaeoclimatology, Palaeoecology*, *414*, 98–115. https://doi.org/10.1016/j.palaeo.2014.08.013

Sial, A. N., Lacerda, L. D., Ferreira, V. P., Frei, R., Marquillas, R. A., Barbosa, J. A., et al. (2013). Mercury as a proxy for volcanic activity during extreme environmental turnover: The Cretaceous-Paleogene transition. *Palaeogeography, Palaeoclimatology, Palaeoecology*, *387*, 153–164. https://doi.org/10.1016/j.palaeo.2013.07.019

Smit, J., Koeberi, C., Claeys, P., & Montanari, A. (2016). Mercury anomaly, Deccan volcanism, and the end-Cretaceous mass extinction. *Comment Geology*, *44*(3), e381. https://doi.org/10.1130/G37683C.1

Stern, G. A., Sanei, H., Roach, P., Delaronde, J., & Outridge, P. M. (2009). Historical interrelated variations of mercury and aquatic organic matter in lake sediment cores from a subarctic lake in Yukon, Canada: Further evidence toward the algal-mercury scavenging hypothesis. *Environmental Science and Technology*, *43*(20), 7684–7690. https://doi.org/10.1021/es902186s

Suan, G., Rulleau, L., Mattioli, E., Suchéras-Marx, B., Rousselle, B., Pittet, B., et al. (2013). Palaeoenvironmental significance of Toarcian black shales and event deposits from southern Beaujolais, France. *Geological Magazine*, *150*(4), 728–742. https://doi.org/10.1017/S0016756812000970

Them, T. R. II, Jagoe, C. H., Caruthers, A. H., Gill, B. C., Grasby, S. E., Gröcke, D. R., et al. (2019). Terrestrial sources as the primary delivery mechanism of mercury to the oceans across the Toarcian Oceanic Anoxic Event (Early Jurassic). *Earth and Planetary Science Letters*, *507*, 62–72. https://doi.org/10.1016/j.epsl.2018.11.029

Thibodeau, A., Ritterbush, K., Yager, J. A., West, J., Ibarra, Y., Bottjer, D. J., et al. (2016). Mercury anomalies and the timing of biotic recovery following the end-Triassic mass extinction. *Nature Communications*, *7*(1), 11147. https://doi.org/10.1038/ncomms11147

Tissot, B. P., & Welte, D. H. (1984). *Petroleum formation and occurrence* (2nd ed., p. 699). Berlin: Springer-Verlag. https://doi.org/10.1007/978-3-642-87813-8

Wang, X., Cawood, P. A., Zhao, L., Grasby, S. E., Chen, Z. Q., & Zhang, L. (2019). Global mercury cycle during the end-Permian mass extinction and subsequent Early Triassic recovery. *Earth and Planetary Science Letters*, *513*, 144–155. https://doi.org/10.1016/j.epsl.2019.02.026

Winterer, E. L., & Bosellini, A. (1981). Subsidence and sedimentdtion on a Jurassic passive continental margin, southern Alps, Italy. *American Association of Petroleum Geologists Bulletin*, *65*, 3944421.

Wood, J. M., Kennedy, F. S., & Rosen, C. G. (1968). Synthesis of methyl-mercury compounds by extracts of a methanogenic bacterium. *Nature*, *220*(5163), 173–174. https://doi.org/10.1038/220173a0

Zintwana, M. P., Cawthorn, R. G., Ashwal, L. D., Roelofse, F., & Cronwright, H. (2012). Mercury in the Bushveld Complex, South Africa, and the Skaergaard Intrusion, Greenland. *Chemical Geology*, *320*, 147–155.